ON THE DYNAMICS OF A TWO-PHASE, NONEVAPORATING SWIRLING JET

T. W. PARK[1], V. R. KATTA†[1] and S. K. AGGARWAL[2]‡

[1]Wright-Patterson Air Force Base, OH 45430, U.S.A.
[2]Department of Mechanical Engineering, University of Illinois at Chicago, Chicago, IL 60607, U.S.A.

Abstract—In this paper, we present direct numerical simulation of a droplet-laden swirling jet, and examine the effects of swirl and two-phase momentum coupling on the jet dynamics and structural characteristics. A time-dependent, multi-dimensional, two-phase algorithm is developed for the simulation. Results for the single-phase swirling jet at a Reynolds number of 800 indicate that the dynamics of large-scale structures are strongly affected by the degree of swirl imparted to the incoming flow. For low and intermediate swirl intensities, the vortex rings roll up closer to the nozzle exit, their frequency increases, and pairing interactions become progressively stronger as the swirl number (S) is increased. Thus, the addition of swirl to a transitional jet appears to modify its vortex dynamics in a way that enhances the beneficial effects of both swirl and vortex structures on the shear layer growth and entrainment. For a strongly swirling jet, the presence of a central stagnant zone and recirculation bubble causes a dramatic increases in the jet spreading angle, and this has a very dramatic effect on vortex dynamics. Based on a detailed visualization of the dynamic structure, we speculate that vortex structures in turn play an important role in determining the location and size of recirculation bubble. Results for the two-phase swirling jet indicate that for a mass loading ratio of unity, the jet dynamic and time-averaged behavior are strongly affected by both the interphase momentum coupling and swirl intensity. For a nonswirling two-phase jet, the momentum coupling modifies the dynamics of large vortex structures, including their roll-up location and frequency, which leads to enhanced mixing and entrainment of colder fluid into the shear layer. In contrast, for weakly and moderately swirling two-phase jets ($S < 0.5$), the momentum coupling reduces the shear layer growth, as well as mixing and entrainment rate. As the swirl number is increased, the effect becomes progressively stronger, manifested by the reduced rate of decay of gas velocity and temperature along the jet axis. In addition, the relation between roll-up frequency and swirl is modified in that the frequency increases with S for a single-phase jet, while it becomes independent of S for the corresponding two-phase jet. Consequently, the vortex pairing interactions, which are responsible for enhanced mixing and entrainment for single-phase swirling jets, are suppressed for two-phase jets. For strongly swirling two-phase jets ($S > 0.5$), the effect of momentum coupling becomes even more dramatic. Results for $S = 0.75$ indicate a drastic reduction in the size of the recirculation bubble for the two-phase jet. © 1998 Elsevier Science Ltd. All rights reserved

Key Words: two-phase flow, swirling jet, large-scale structures, transient behavior

1. INTRODUCTION

Swirling jet flows are utilized in a wide range of applications. By imparting swirl to the incoming flow, the structure of both nonreacting and reacting flows can be changed in a dramatic manner (Lilley 1977). The structure of swirling jet, for example, is strongly affected by the degree of swirl, characterized by a swirl number (S) which is defined as the ratio of axial flux of swirl or azimuthal momentum to that of axial momentum. For a weakly swirling nonreacting jet ($S < 0.4$), the jet growth, entrainment and decay are enhanced progressively as S is increased. For a corresponding strongly swirling jet ($S > 0.5$), the behavior changes more dramatically due to the formation of a recirculation bubble. In combustion applications, the recirculation bubble perhaps represents the most significant and useful effect of swirl, as it plays a central role in flame stabilization and enhanced combustor performance.

†Present address: Innovative Scientific Solutions, Inc., Dayton, OH 45430, U.S.A.
‡To whom all correspondence should be addressed. Phone: (312) 996-2235; fax: (312) 413-0447; e-mail: ska@uic.edu.

Extensive research efforts have been expended in understanding and characterizing the effects of swirl in nonreacting and reacting flows (Lilley 1977; Ribeiro and Whitelaw 1980; Leschziner and Rodi 1984). A commonly used configuration in both experimental and computational studies involves a confined or free swirling jet. Most of these studies, however, deal with the time-averaged behavior of swirling single-phase (Leschziner and Rodi 1984; Dellenbach *et al.* 1988; Durst and Wennerberg 1991) and two-phase jets (Sommerfeld and Qui 1993). The transient aspects, particularly those associated with large-scale vortex structures, have not been examined, although these structures have been shown to have a dominant effect on the near jet flow dynamics of non-swirling jets. Numerous experimental and numerical studies (Crow and Champagne 1971; Yule 1978) have shown that toroidal vortex rings form periodically in the near field of round jets and convect downstream. These axisymmetric structures roll around due to the inhomogeneous flow field, and may also undergo pairing interactions, depending on the flow conditions, such as initial disturbance level and other experimental conditions. In addition, their dynamics can be modified significantly by external forcing (Reynolds and Bouchard 1981). There are also other mechanisms that can modify their temporal and spatial growth characteristics. These include acoustic (pressure) fluctuations (Kailasanath *et al.* 1989), which can modify the dominant frequency associated with large scale structures, compressibility effects (Shau *et al.* 1993), and density variations caused by a variation in temperature or molecular weight (Subbarao and Cantwell 1992). Yet another mechanism that may alter the dynamics of large-scale structures pertains to the effect of swirl, which induces a body force in the radial momentum equation, and an adverse pressure gradient in the axial direction. For weakly swirling jets, the axial adverse pressure gradient caused by swirl can modify the processes of vortex roll-up and pairing interactions. For strongly swirling jets, the jet spreading and recirculation zone created by the swirl effect can have a more dramatic effect on the dynamics of vortex rings. To our knowledge, these aspects dealing with the dynamic interactions between large scale structures and swirl, and those between large structures and droplets in a swirling shear flow, have not been investigated in previous studies.

In this paper, we present a numerical simulation of a droplet-laden swirling jet. The major objective of this study is to investigate the dynamics of large-scale structures under different swirl conditions, and their interactions with the droplets injected in the shear layer of an axisymmetric swirling jet. A direct numerical solver without any turbulence or subgrid model is employed. The simulation first examines the dynamics of vortex rings and their interactions with the swirling flow field in a transitional heated jet. Then, a droplet-laden swirling jet is simulated in order to examine the effects of two-phase momentum coupling on the jet dynamics and structural behavior. The jet Reynolds number based on a jet velocity of 5.0 m/s, diameter 25.4 mm, and kinematic viscosity of heated jet fluid is 800. In our earlier study (Aggarwal *et al.* 1996), the dynamics of a nonswirling two-phase jet were investigated, and it was shown that the shear layer stability and vortex dynamics can be modified significantly by controlling the droplet injection characteristics. The present study extends that work to a swirling two-phase jet, and examines the effects of both swirl and two-phase momentum coupling on its dynamic and time-averaged structure.

2. PHYSICAL– NUMERICAL MODEL

A cartoon of the two-phase swirling jet investigated in the present study is shown in figure 1. It consists of a central swirling jet which is a two-phase mixture of air and liquid fuel (n-heptane) droplets and a low-speed annular air flow. The jet at axial velocity of 5.0 m/s and temperature of 1200 K is issuing into a co-flow with a velocity of 0.2 m/s without swirl and temperature of 294 K. Note that the use of high jet temperature is based on the consideration that we plan to investigate an evaporating spray in a subsequent study. In the present study, a nonevaporating spray is simulated in order to examine the effects of two-phase momentum coupling in the near region of a swirling jet. The jet–shear-layer instability is primarily of the Kelvin–Helmholtz type (Aggarwal *et al.* 1996).

The numerical model is based on solving the time-dependent, two-phase equations in an axisymmetric geometry. The unsteady, axisymmetric governing equations in cylindrical (z, r)

coordinates for a droplet-laden swirling jet are:

$$\frac{\partial(\rho\Phi)}{\partial t} + \frac{\partial(\rho u\Phi)}{\partial z} + \frac{\partial(\rho v\Phi)}{\partial r} = \frac{\partial}{\partial z}\left(\Gamma^{\Phi}\frac{\partial\Phi}{\partial r}\right) + \frac{\partial}{\partial r}\left(\Gamma^{\Phi}\frac{\partial\Phi}{\partial z}\right) - \frac{\rho v\Phi}{r} + \frac{\Gamma^{\Phi}}{r}\frac{\partial\Phi}{\partial r} + S_G^{\Phi} + S_L^{\Phi}. \qquad [1]$$

The general form of [1] represents the continuity, three momentum, and energy conservation equations depending on the variable used for Φ. The transport coefficients Γ^{Φ} and the source terms S_G^{Φ} and S_L^{Φ} that appear in the governing equations are listed in table 1. Note that the equations in table 1 correspond to an evaporating two-phase flow. For the present study, which simulates a nonevaporating two-phase flow, the species equations are not considered, and droplet vaporization rate ($\dot{m}_k$) is taken identically equal to zero. The transport coefficients Γ^{Φ} and source terms contain the fluid properties such as viscosity (μ), thermal conductivity (λ), and specific heat (C_p). They are considered functions of temperature and species concentration.

The effect of dispersed phase on gas-phase properties is incorporated through the source/sink terms (S_L^{Φ}), representing the exchange of momentum between the gas and dispersed phases. In order to evaluate these terms, it is necessary to establish droplet trajectories. The Lagrangian approach is employed to solve the liquid-phase governing equations for the dynamics of each droplet group. The spray is characterized by a discrete number of droplet groups, distinguished by their injection location, initial size, and time of injection. A droplet group in a Lagrangian treatment represents a characteristic group containing a finite number of droplets. Since an axisymmetric configuration is analyzed, the liquid properties are implicitly averaged in the azimuthal direction and the number of droplets associated with each characteristic group represents droplets uniformly distributed in an annular ring. The equations governing the variation of position and velocity of each droplet are as follows:

$$\frac{\mathrm{d}z_k}{\mathrm{d}t} = u_k$$

$$\frac{\mathrm{d}y_k}{\mathrm{d}t} = v_k \qquad [2]$$

$$\frac{\mathrm{d}u_k}{\mathrm{d}t} = \frac{3C_D\rho_G}{4d_k\rho_k}|u - u_k|(u - u_k) + \left(\frac{\rho_G}{\rho_k} - 1\right)g$$

$$\frac{\mathrm{d}v_k}{\mathrm{d}t} = \frac{3C_D\rho_G}{4d_k\rho_k}|v - v_k|(v - v_k) + \frac{w_k^2}{y_k} \qquad [3]$$

$$\frac{\mathrm{d}w_k}{\mathrm{d}t} = \frac{3C_D\rho_G}{4d_k\rho_k}|w - w_k|(w - w_k) - \frac{v_k w_k}{y_k}$$

where

$$C_D = \frac{24}{\mathrm{Re}_k}\left(1 + \frac{\mathrm{Re}_k^{2/3}}{6}\right) \qquad [4]$$

$$\mathrm{Re}_k = \frac{\rho_G\{(u - u_k)^2 + (v - v_k)^2 + (w - w_k)^2\}^{1/2}d_k}{\mu_G}. \qquad [5]$$

In the above equations, z_k and y_k are, respectively, the instantaneous axial and radial locations of a droplet group, while u_k, v_k, and w_k are, respectively, its axial, radial, and azimuthal velocity components. Further, d_k, ρ_k, and Re_k are, respectively, the droplet size, material density and Reynolds number, whereas ρ_G and μ_G are the gas density and viscosity, respectively. In the present simulation, we consider nonevaporating n-heptane droplets. In a subsequent study, we plan to extend the analysis to evaporating droplets. The density of n-heptane fuel is assumed to be 649.4 kg/m³, which yields a value of more than 100 for the ratio of droplet density to gas density, with the latter value based on an average gas temperature of 750 K. This sufficiently large density ratio allows us to neglect the Basset force, pressure gradient and other contri-
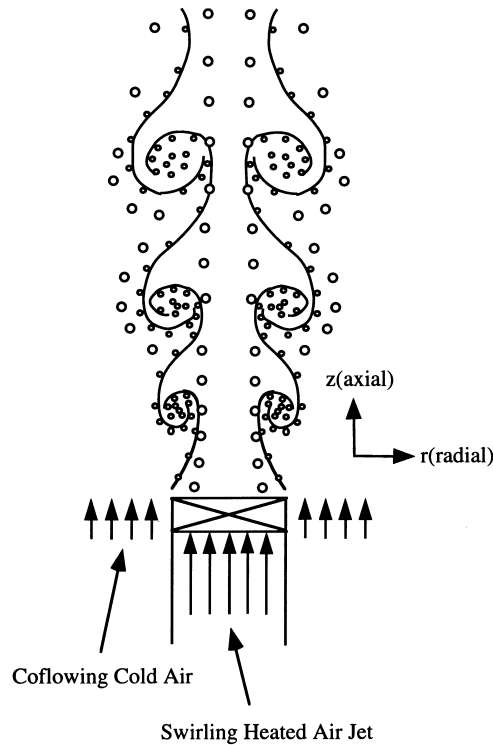
Figure 1. Schematic of a droplet-laden swirling jet..

butions from flow non-uniformities, and consider only the quasi-steady drag and gravity forces in [3].

The numerical solution of the unsteady two-phase equations employs an implicit algorithm for solving the gas-phase equations, and an explicit Runge–Kutta procedure for the liquid-phase equations. The finite-difference forms of the momentum equations are obtained using an implicit QUICKEST scheme (Leonard 1979), while those of energy equations are obtained using a hybrid scheme of upwind and central differencing (Spalding 1972). A 'finite control volume' approach with a nonuniform staggered-grid system is utilized. An orthogonal grid having expanding cell sizes in both the axial and the radial direction is employed. An iterative ADI (Alternative Direction Implicit) technique is used for solving the resulting sets of algebraic equations. At every time step, the pressure field is calculated by solving all the pressure Poisson equations simultaneously and utilizing the LU (lower and upper diagonal) matrix decomposition technique.

Axisymmetric calculations are made on a physical domain of $400 \times 150 \, \text{mm}^2$ utilizing a 151×61 nonuniform grid system. The computational domain is bounded by the axis of symmetry and an outflow boundary in the radial direction and by the inflow and another out-flow boundary in the axial direction. The outer boundaries in the z and r directions are located sufficiently far from the nozzle exit (16 nozzle diameters) and the axis of symmetry (six nozzle diameters), respectively, to minimize the propagation of boundary-induced disturbances into the region of interest (seven and two nozzle diameters in the axial and radial directions, respect-ively). A flat profile for axial velocity and a linear profile for swirl velocity (swirl velocity being a linearly increasing function of radius) are used at the inflow boundary. It is important to mention that, for a given swirl number, one can employ different swirl velocity profiles at the inflow boundary, and this may affect the jet development. However, a linear velocity profile pro-vides a good approximation to the real situation, and has often been used in computational stu-dies (Ribeiro and Whitelaw 1980; Leschziner and Rodi 1984). A zero-gradient boundary condition with an extrapolation procedure with weighted zero- and first-order terms is used to estimate the flow variables at the outflow boundary. The weighting functions are selected using

Table 1. Transport coefficients and source terms appearing in gas-phase governing equations

Equations	Φ	Γ^Φ	S_G^Φ	S_T^Φ
Continuity	1	0	0	$\sum_k n_k\dot{m}_k$
Axial momentum	u	μ	$-\dfrac{\partial p}{\partial z}+(\rho_0-\rho)g+\dfrac{\partial}{\partial z}\left(\mu\dfrac{\partial u}{\partial z}\right)+\dfrac{\partial}{\partial r}\left(\mu\dfrac{\partial v}{\partial z}\right)+\dfrac{\mu}{r}\dfrac{\partial v}{\partial z}-\dfrac{2}{3}\left[\dfrac{\partial}{\partial z}\left(\mu\dfrac{\partial u}{\partial z}\right)+\dfrac{\partial}{\partial z}\left(\mu\dfrac{\partial v}{\partial r}\right)+\dfrac{\partial}{\partial z}\left(\mu\dfrac{v}{r}\right)\right]$	$\sum_k\left(n_k\dot{m}_k u_k-n_k M_k\dfrac{du_k}{dt}\right)$
Radial momentum	v	μ	$-\dfrac{\partial p}{\partial r}+\dfrac{\partial}{\partial z}\left(\mu\dfrac{\partial u}{\partial r}\right)+\dfrac{\partial}{\partial r}\left(\mu\dfrac{\partial v}{\partial r}\right)+\dfrac{\mu}{r}\dfrac{\partial v}{\partial r}-2\mu\dfrac{v}{r^2}+\rho\dfrac{w^2}{r}-\dfrac{2}{3}\left[\dfrac{\partial}{\partial r}\left(\mu\dfrac{\partial u}{\partial z}\right)+\dfrac{\partial}{\partial r}\left(\mu\dfrac{\partial v}{\partial r}\right)+\dfrac{\partial}{\partial r}\left(\mu\dfrac{v}{r}\right)\right]$	$\sum_k\left(n_k\dot{m}_k v_k-n_k M_k\dfrac{dv_k}{dt}\right)$
Swirl momentum	w	μ	$-\left(\dfrac{\mu}{r^2}+\rho\dfrac{v}{r}+\dfrac{1}{r}\dfrac{\partial\mu}{\partial r}\right)w$	$\sum_k\left(n_k\dot{m}_k w_k-n_k M_k\dfrac{dw_k}{dt}\right)$
Mass fraction of fuel	Y_f	ρD_{f-N_2}	0	$\sum_k n_k\dot{m}_k$
Mass fraction of other species	Y_i $(i=1\text{-}N_s,\ i\neq f)$	ρD_{i-N_2}	0	0
Energy	H	$\dfrac{\lambda}{C_p}$	0	$\sum_k n_k\dot{m}_k(h_{fs}-l_{k,\text{eff}})$

the trial-and-error approach, and the main criterion used is that the vortices crossing the out-flow boundary leave smoothly without being distorted. For the given flow conditions, a steady-state solution was first obtained by neglecting the unsteady terms in the governing equations. Then, the unsteady two-phase swirling jet simulations were performed using the previously obtained steady-state solution as the initial flow condition.

The liquid-phase equations governing the position of each droplet group are advanced in time by a second-order accurate Runge-Kutta method. Since the gas-phase solution employs an implicit procedure, the temporal step size used for integrating the liquid-phase equations is usually smaller than that for gas-phase equations. An automatic procedure is implemented in order to select an optimum liquid-phase time step. The procedure to advance the two-phase solution over one gas-phase time step is as follows. Using the known gas-phase properties, the liquid-phase equations are solved over the specified number of liquid-phase subcycles. A third-order accurate Lagrangian polynomial method is used for interpolating the gas-phase properties from the nonuniform fixed grid to the droplet characteristic location. It should be noted that the interpolation scheme for the gas-phase velocities (u, v and w) is based on their respective grid cells because of the use of a staggered grid in gas-phase calculation. The droplet properties are updated after every liquid-phase subcycle. Also, during each subcycle, the liquid-phase source terms appearing in the gas-phase equations are calculated at the characteristic location, and then distributed to the surrounding gas-phase grid points. These source terms are added at each gas-phase grid points during one gas-phase time step and then used in the implicit solution of the gas-phase equations. It is also important to note that the integration of droplet equations [3] in cylindrical coordinates require special care near the axis of symmetry, where a specular boundary condition is imposed. This implies that, as a droplet approaches the left boundary, it is replaced by another droplet entering the domain at the reflected angle.

Numerical validation studies for both single-phase and two-phase jets, as well as for low-speed diffusion flames, employing different grids and temporal step sizes have been reported previously (Aggarwal *et al.* 1996; Katta *et al.* 1994). Some additional results showing grid independence are depicted in figure 2. The time-history of gas velocity computed for two different grid sizes, 151×61 and 226×91 for nonswirling and swirling jets is plotted in figure 2(a) and 2(b), while the profiles of time-averaged velocity along the jet axis for three different swirl numbers are plotted in figure 2(c). Since a nonuniform grid is employed with grid lines clustered near the shear layer to resolve the steep gradients of the dependent variables, additional grid points in the 226×91 grid are placed near the shear layer, thus effectively reducing the grid density for this grid by nearly 100% compared to the 151×61 grid. The time-history plots of gas velocity clearly depict the highly periodic nature of jet vortex rings associated with the Kelvin–Helmholtz instability. For the nonswirling jet, the Strouhal number associated with this instability obtained from the fast Fourier transform of axial velocity is 0.33, which agrees with the reported experimental range of 0.25–0.5 (Hussain and Hussain 1983). The aspects pertaining to the dynamic and time-averaged jet behavior for different swirl numbers are discussed in the next section. An important observation here is that the 151×61 grid is able to capture the periodic behavior, including the frequency and phase of vortex structures, as well as the time-averaged structure of both nonswirling and swirling jets.

3. RESULTS

The swirl number is defined as

$$S = \frac{1}{r_0} \frac{\int_0^{r_0} uwr^2 \, \mathrm{d}r}{\int_0^{r_0} u^2 r \, \mathrm{d}r} \qquad [6]$$

where r_o is the radial extent of computational domain, r is the radial coordinate, and u and w are, respectively, the gas axial and azimuthal velocity components. This definition treats S as a function of axial distance. Thus, at the inflow boundary r_0 becomes equal to the jet radius.

First, we examine the dynamics of single-phase swirling jets at different swirl numbers (S). The objective is to understand and characterize the dynamic interactions between swirl and
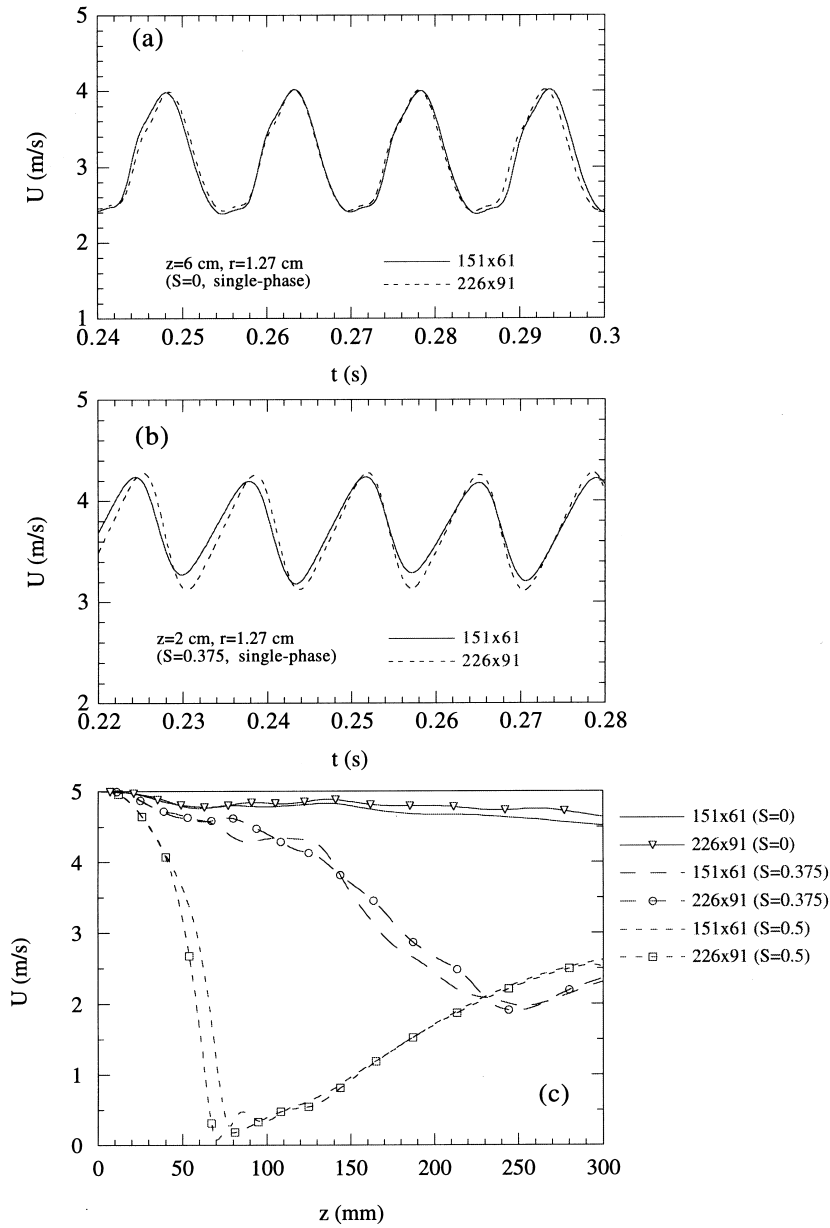
Figure 2. Time-history plots of centerline gas velocity (a and b) and axial profiles of time-averaged centerline gas velocity (c) for nonswirling and swirling (swirl number $S = 0.375$) jets obtained by using two different grid sizes..

large-scale structures, and the effects of these interactions on the jet behavior. Since the jet dynamics and structural characteristics are strongly influenced by the presence of both swirl and large scale structures, it is of interest to examine how the vortex dynamics are affected by swirl, and how the distribution of swirl and its decay rate are modified by vortex structures. The latter effect is important since the swirl decay rate determines the pressure distribution, and thereby the jet gross behavior, especially the onset, location and extent of the recirculation bubble at high swirl numbers. The above interactions are examined by employing flow visualization (snapshots of the flow field), as well as the instantaneous and time-averaged properties.

Figure 3 shows some representative snapshots of the flow field for different swirl numbers. In each snapshot, we plot instantaneous iso-temperature contours on the right, and streaklines on the left. Simulations for the nonswirling jet indicate the presence of well-organized vortex rings. Toroidal vortex rings roll up periodically near $z = 4$ cm ($z/D = 1.6$) from the nozzle exit,

convect downstream, and undergo a weak pairing interaction near $z = 16$ cm. The snapshot for $S = 0$ clearly indicates a vortex roll-up occurring near $z = 4$ cm, and a pairing interaction near $z = 16$ cm. These results were confirmed by the fast Fourier transform of axial velocity recorded at several axial locations, shown in figure 4(a), which yields dominant frequencies of 64 and 32 Hz corresponding to the roll-up and merging frequencies, respectively. Results for $S = 0.375$, figure 3, indicate a more dramatic effect of swirl on the dynamics of large scale structures. First of all, the vortex roll-up location is shifted upstream and the frequency is increased from 64 to 75 Hz compared to the nonswirling case. Second, the vortex pairing becomes a prominent feature of shear layer dynamics in the near jet region, which, we speculate, is caused by the adverse pressure gradient effect of swirl. Since, the pressure increases along the centerline for the swirling case, the centerline velocity for the swirling jet decays faster compared to that for the nonswirling jet. This is indicated clearly in figure 5(a), which shows the variation of time-averaged gas velocity along the centerline for different swirl numbers. As a result, the leading toroidal vortex is slowed down, causing a well-organized pairing interaction to occur near $z = 7$ cm. The faster decay of centerline velocity also causes the occurrence of second vortex pairing near $z = 12$ cm. The processes of shear layer roll-up and pairing interactions for $S = 0.375$ are clearly depicted in figure 3. The corresponding frequencies, obtained from the fast Fourier transform of axial velocity and displayed in figure 4(b), are 74, 37, and 19 Hz, respectively. The occurrence of multiple vortex pairings in a swirling jet has an important implication with regard to the effect of swirl–vortex interaction on the jet development and entrainment. Since the presence of multiple vortex pairings is known to enhance shear layer growth and entrainment, the numerical results indicate that the addition of swirl modifies vortex dynamics in a way which further enhances the beneficial effects of swirl.

As the swirl intensity is increased, the above effects become progressively stronger. The increased swirl strength promotes greater jet spreading, mixedness, and reduction of the potential core. In addition, the vortex roll-up occurs earlier (more upstream), and the convecting toroidal vortex slows down considerably, as it moves radially outward (due to jet spreading) and the centerline velocity decays more rapidly. Consequently, with increased swirl, vortex pairings occur earlier and with greater intensity, further promoting shear layer growth and entrainment. For $S = 0.5$, as noted in figure 3, the locations of vortex roll-up and first and second pairing interactions are at approximately $z = 2$, 5, and 8 cm, respectively, compared with the corresponding values of 3, 7, and 10 cm for $S = 0.375$. In addition, the corresponding frequencies are higher and a third pairing interaction is observed for $S = 0.5$; see figure 4(c). The above observations are also confirmed by the axial profiles of time-averaged gas velocity and temperature shown in figure 5. As S is increased, the centerline temperature decreases more rapidly, indicating a pronounced increase in the shear layer growth and entrainment of colder fluid into the hot jet. This is a significant result in that the overall effect of swirl–vortex interaction at low to intermediate swirl intensities ($S < 0.5$) is to augment the effect of each. Note that both the addition of swirl and the presence of large vortex structures are known to enhance shear layer growth and entrainment. Our results indicate that an increase in swirl intensity promotes multiple vortex pairings, which further enhances shear layer growth and entrainment, i.e. large structures augment the effect of swirl and *vice versa*.

A more dramatic effect occurs as the swirl number exceeds 0.5, which represents the onset of recirculation bubble in the jet flow. For $S > 0.5$, a stagnant region develops near the centerline due to the reverse flow caused by adverse pressure gradient, and a toroidal recirculation bubble appears. Both the central stagnation region and recirculation bubble can clearly be seen from the time-averaged velocity vector plots in figure 6. Also notable in this figure is the presence of a secondary recirculation zone for $S = 0.75$, located just upstream of the primary recirculation bubble. The stagnation region and reverse flow are also quite evident in the time-averaged axial velocity profile for $S = 0.75$ given in figure 5. In addition, as noted in figure 6, the jet shear layer for $S = 0.75$ is shifted significantly outward in the radial direction, and exhibits a highly dynamic structure. It is interesting to note that, while at subcritical swirl numbers ($S < 0.5$) toroidal vortices are an intrinsic part of jet dynamics, their existence becomes less obvious at supercritical swirl numbers ($S > 0.5$). Thus, an important issue to be addressed here pertains to the existence and nature of large scale structures for strongly swirling jets, and whether the tran-
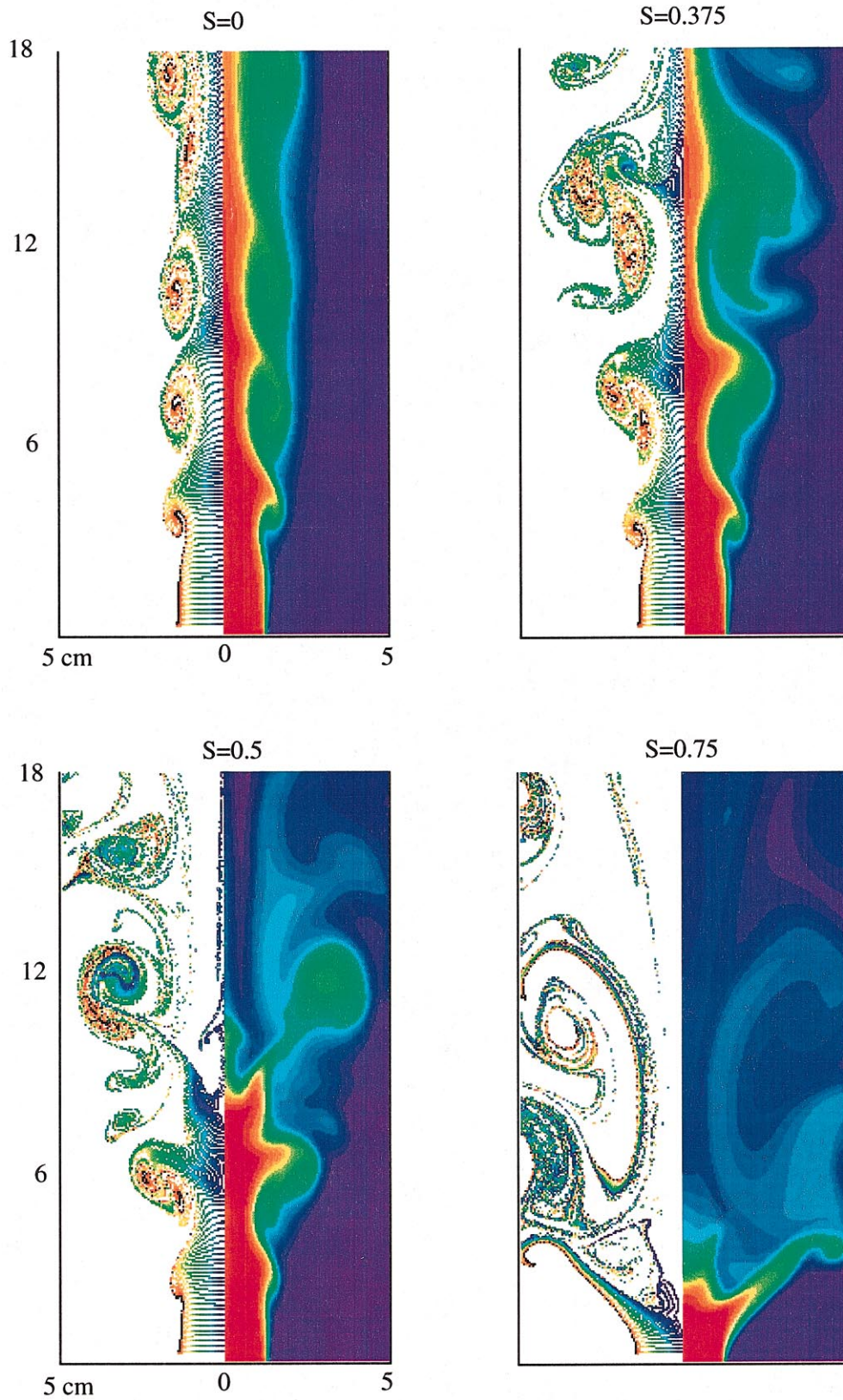
S=0

S=0.375

S=0.5

S=0.75

5 cm

Figure 3. Snapshots of the flow field for a swirling jet without droplets for four different swirl numbers. In each snapshot, iso-temperature contours are plotted on the right-hand side of the symmetric jet, and streaklines on the left. For iso-temperature contours, the red and purple colors represent the highest (1200 K) and the lowest (294 K) temperatures, respectively. The times of the snapshots are 0.21, 0.24, 0.25, 0.2 s for $S = 0$, 0.375, 0.5, and 0.75, respectively..
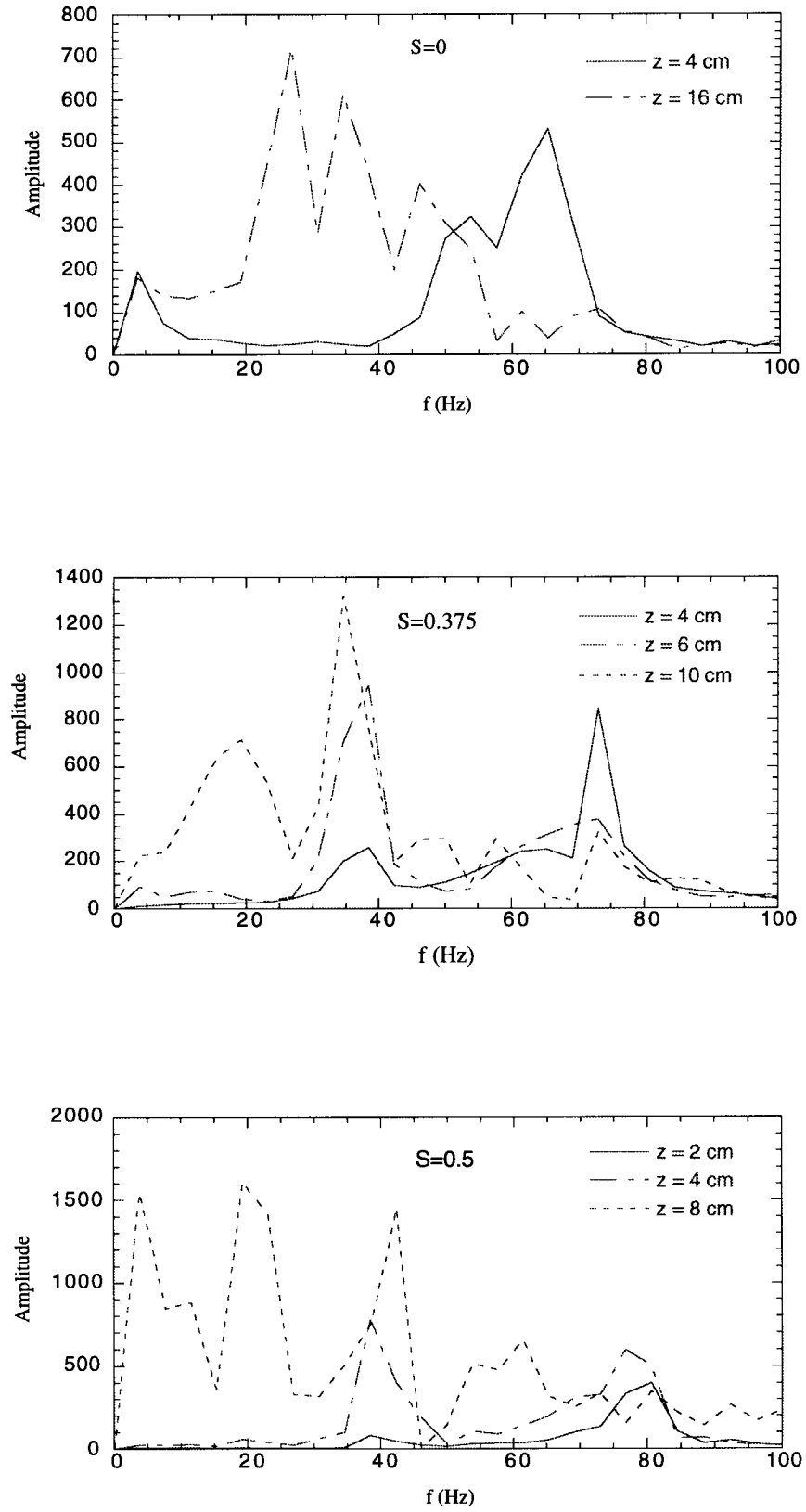
Figure 4. Frequency spectra of axial gas velocity for a swirling jet without droplets for different swirl numbers..
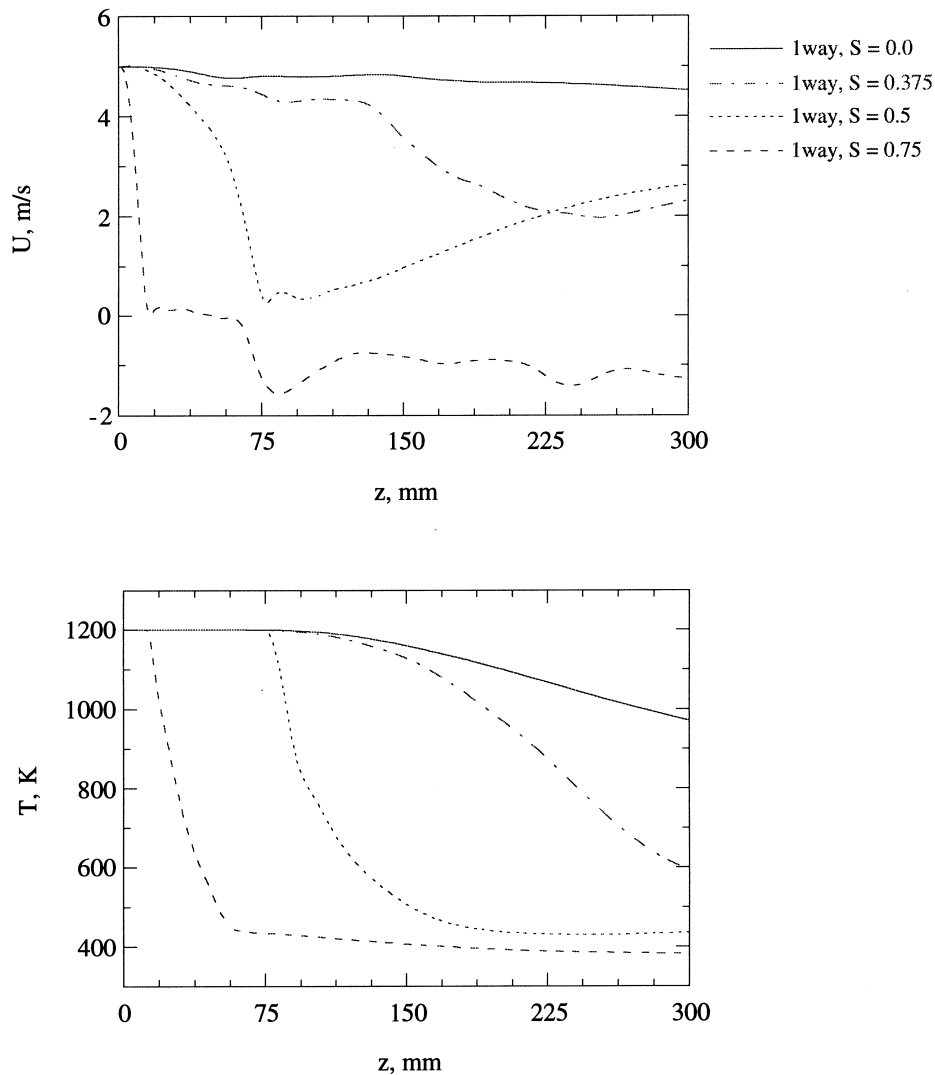
Figure 5. Axial profiles of time-averaged gas velocity and temperature for a swirling jet without droplets for different swirl numbers..

sient jet behavior can be attributed to these structures. One may argue that these structures get destroyed due to the rapid decay of shear and increased mixing in a strongly swirling jet. Based on an extensive visualization of the swirling jet dynamics for $S = 0.75$, we speculate that large vortex structures are still present, though their behavior is markedly different from those for the weakly and moderately swirling jets ($S < 0.5$). The vortex structures for $S = 0.75$ are shifted outward in the radial direction and do not look like the Kelvin–Helmholtz vortex rings that are typically observed in a transitional jet. However, a series of snapshots (not shown) indicated that they do exhibit the processes of roll-up and pairing interactions, though in a significantly less organized manner. The snapshots further indicate that a pair of counter-rotating toroidal vortices (an outer Kelvin–Helmholtz type vortex rotating clockwise and an inner vortex rotating counter-clockwise; the latter may be due to the presence of central stagnation region) is generated periodically. As these vortices convect downstream, they grow in size, and the outer structure rolls around the inner structure since the latter is in a nearly stagnant region. In addition, both outer and inner vortices undergo pairing interactions with other (trailing) outer and inner vortices, respectively. We also speculate, based on the flow visualization and time-averaged velocity vector plots shown in figure 6, that the size and location of recirculation bubble is deter-
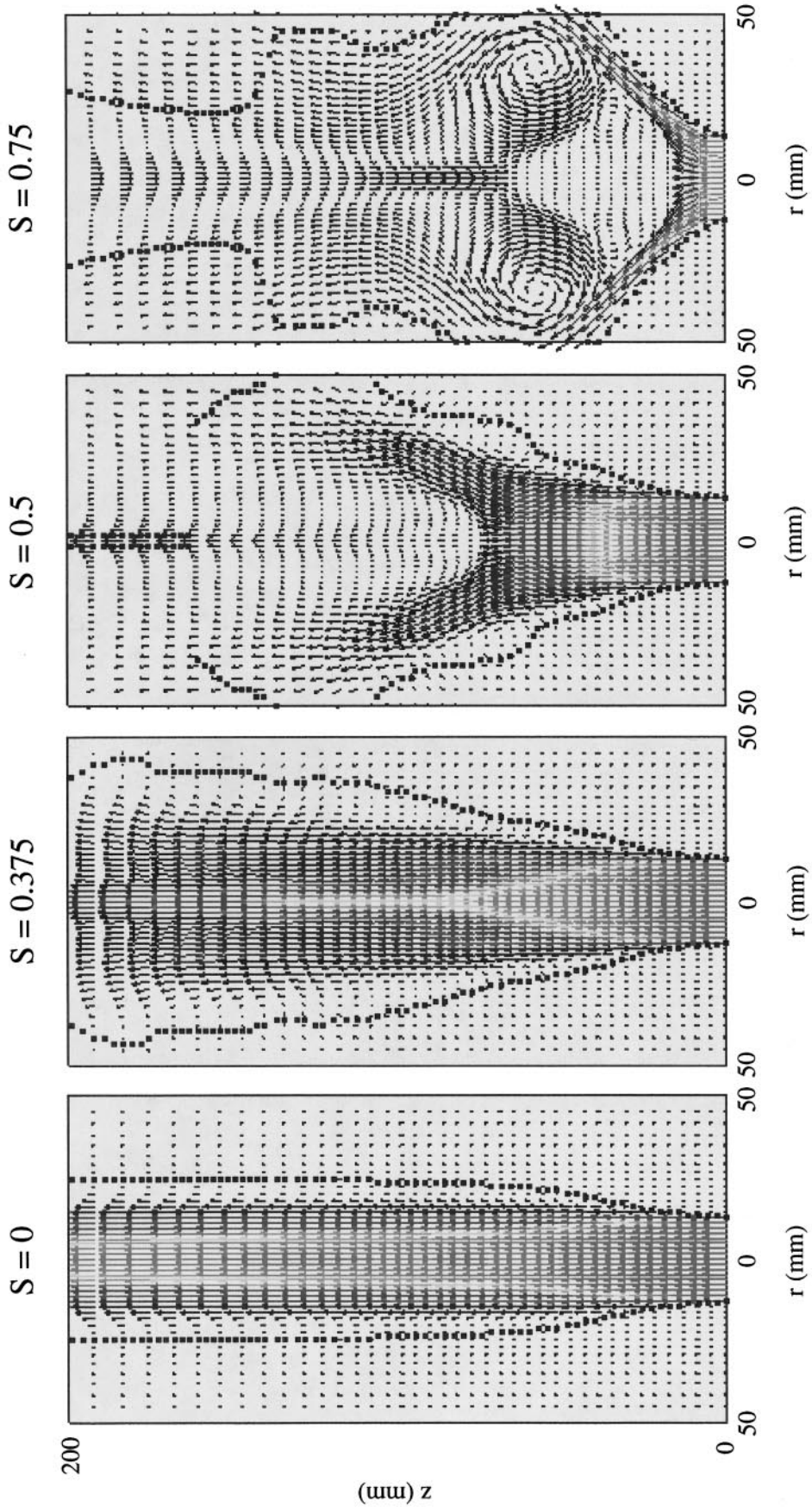
Figure 6. Time-averaged velocity vector plots for a swirling jet without droplets for different swirl numbers..

mined by these dynamic swirl–vortex interactions, and not by the adverse pressure gradient (swirl effect) alone. In other words, due to the effect of swirl, the outer vortex is shifted outward in the radial direction, and its subsequent dynamics as well as those of the inner vortex are determined by the swirling flow field. These vortices in turn play a major part in determining the location of recirculation zone; it appears that the recirculation zone is established at a location where the outer vortex structure is pulled in radially.

3.1. *Two-phase momentum coupling effects*

We now examine the effects of two-phase momentum coupling on the dynamics and time-averaged characteristics of a droplet-laden swirling jet. Droplets of a given size are injected from the nozzle rim, and their motion is followed by integrating [2] and [3] using a second-order Runge–Kutta scheme. At low mass loadings, the effect of droplets on the jet dynamics is negligible, although their motion and concentration field are strongly influenced by the rotating toroidal vortices. As the dispersed-phase mass loading is increased, the effects due to the exchange of mass, momentum, and energy between the phases become increasingly important. In the present study, a nonevaporating two-phase jet is considered in order to isolate momentum coupling effects from those due to mass and energy coupling. These effects depend on several parameters, including liquid-to-air mass loading ratio and injection characteristics such as initial droplet size, location, and velocity. For the present study, we consider mass loading of unity† and initial droplet diameter of 100 μm, with the droplets injected in the shear layer with axial velocity the same as the jet velocity, and zero radial and azimuthal velocities. Note that the choice of droplet diameter is based on the consideration that it yields a Stokes number of near unity for the nonswirling jet. The Stokes number here is defined as the ratio of droplet response time to a characteristic flow time, the latter based on the dominant vortex frequency. Several experimental (Longmire and Eaton 1992) and numerical studies (Chung and Troutt 1988; Uthuppan *et al.* 1994; Park *et al.* 1996) have shown that the interaction of large structures with droplets is maximized near a Stokes number of unity.

Flow visualization is used to assess qualitatively the effects of dispersed phase on the dynamics of large-scale structures under different swirl conditions. In the following discussion, case A refers to single-phase jets, while case B refers to two-phase jets. Figure 7 depicts representative snapshots of the flow field for different swirl numbers. For these results, a droplet group is introduced every tenth computational time step, and the computations are performed for a total of 10,000 time steps. Thus, there are 1000 droplet groups for the two-phase results shown in figure 7. Comparison of the snapshots, for nonswirling ($S = 0$) single-phase and two-phase jets, given in figures 3 and 7, respectively, indicates that the vortex roll-up location, dynamics, and pairing interactions are strongly modified due to momentum coupling. In addition, it is observed that for the two-phase jet (case B), the vortex structures are stronger and entrain more low-speed (colder) fluid compared to those for the single-phase jet (case A). The comparison of snapshots for swirling jets also indicates a significant modification of vortex dynamics due to the momentum coupling effect. For low to moderate swirl numbers ($S < 0.5$), the vortex pairing is a prominent feature of jet dynamics for case A, while it is not observed for case B. For the strong swirl case ($S = 0.75$), an important effect of two-phase momentum coupling is a drastic reduction in the size of recirculation bubble, even though the central stagnation region still exists. This can be seen more clearly in terms of time-averaged velocity vector plots in figure 11. The effect of momentum coupling on the time-averaged structure is discussed in the following section.

The above observations are confirmed by obtaining the spectral and time-averaged properties for the two cases. Figure 8 shows the time-history of gas-phase axial velocity for single-phase and two-phase jets at different swirl numbers. Results of the fast Fourier transform of these axial-velocity histories are depicted in figures 4 and 9. As discussed earlier, for single-phase jets with low to moderate swirl numbers ($S < 0.5$), processes of shear layer roll-up and vortex formation are well organized. In addition, the roll-up frequency increases and pairing interactions

---

†In an earlier study (Aggarwal *et al.* 1996) it was shown that at unity mass loading, two-phase momentum coupling has a significance influence on the jet dynamics and structural characteristics.
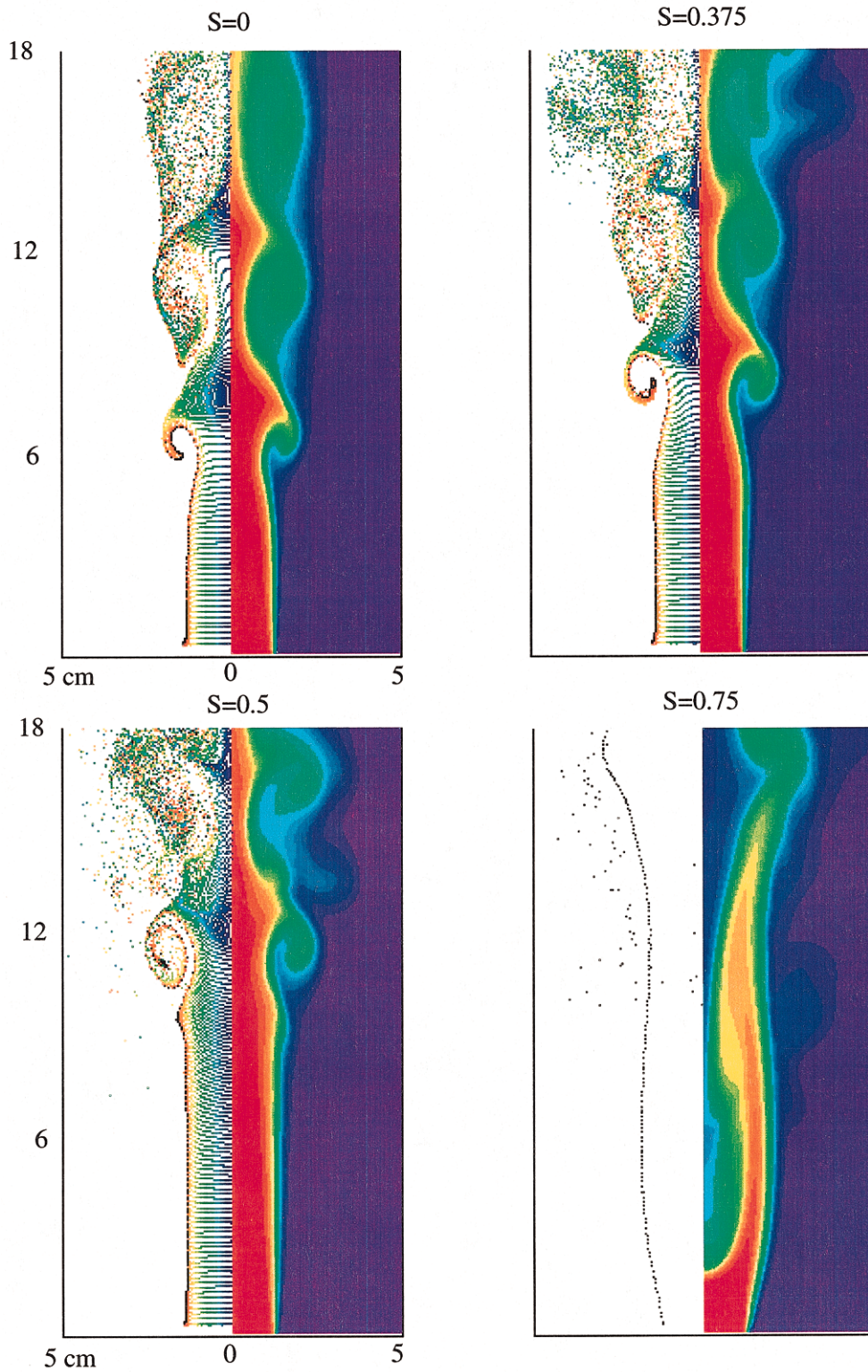
Two-way Coupling

Figure 7. Snapshots of the flow field for a swirling jet with droplets. In each snapshot, iso-temperature contours are plotted on the right-hand side of the symmetric jet, and streaklines on the left. For iso-temperature contours, the red and purple colors represent the highest (1200 K) and the lowest (294 K) temperatures, respectively..
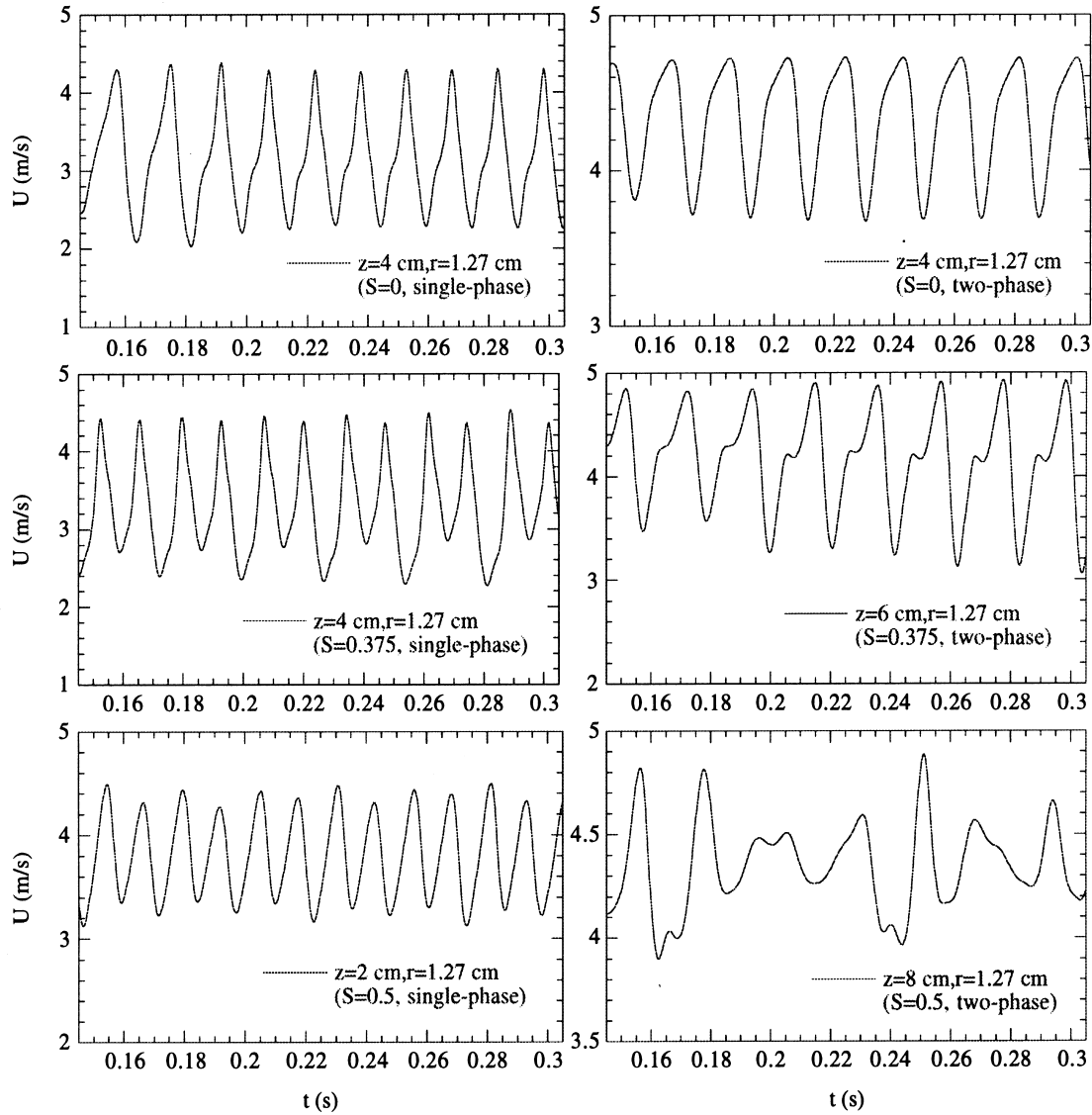
Figure 8. Time history of gas-phase axial velocity for single-phase and two-phase jets with different swirl numbers..

become more prominent as the swirl number is increased. These results are quite evident in figure 4; the roll-up frequencies are 64, 72, and 80 Hz for $S = 0$, 0.375, and 0.5, respectively. Also noteworthy in figure 4 are the first and second pairing interactions at frequencies of 36 and 18 Hz respectively, for $S = 0.375$, and at 40 and 20 Hz respectively, for $S = 0.5$. In contrast, for the corresponding two-phase jets (case B), the shear layer dynamics are relatively less organized, and the roll-up frequency decreases and becomes independent of the swirl number. As indicated in figures 8 and 9, the roll-up frequency is 50 Hz for $S = 0$, 0.375, and 0.5. Another important observation from figure 9 is the absence of pairing interactions for case B, which is also evident in figure 7. This is attributable to the fact that the interphase momentum coupling modifies the distribution of swirl intensity in the axial direction, resulting in a decrease of adverse pressure gradient and jet spreading angle. As noted earlier, the adverse pressure gradient caused by swirl is responsible for the enhanced vortex pairings in single-phase jets. For corresponding two-phase jets, there is a transfer of azimuthal momentum from the gas phase to the droplets, which reduces swirl intensity near the nozzle. Further downstream, however, the momentum is trans-
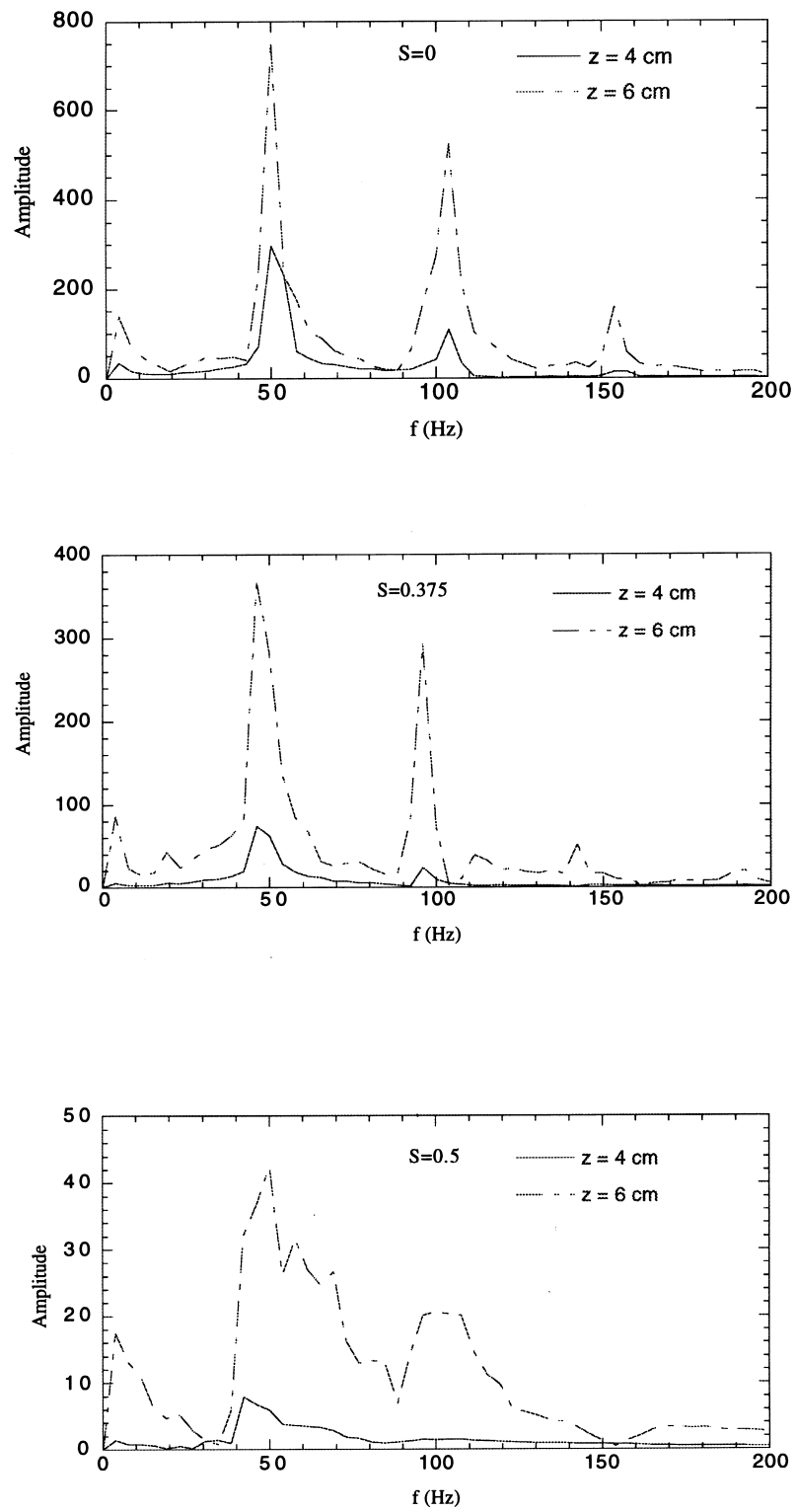
Figure 9. Frequency spectra of axial gas velocity for a swirling jet with droplets for different swirl numbers..

ferred from droplets to gas phase, increasing the gas-phase swirl intensity. The resulting redistribution of swirl intensity reduces the adverse pressure gradient for the two-phase jet. This was confirmed by plotting the time-averaged azimuthal velocity contours (not shown) and axial velocity vectors, shown in figure 11. As a consequence, the vortex pairing, which is prominent feature of moderately swirling ($S < 0.5$) single-phase jets, is not observed for corresponding two-phase jets.

3.2. *Momentum coupling effect on the time-averaged jet structure*

The effect of two-phase momentum coupling on the time-averaged jet behavior is depicted in figures 10 and 11. In figure 10, the time-averaged axial gas velocity and temperature are plotted along the jet centerline, while figure 11 shows the time-averaged velocity vectors for different swirl numbers. The important observation from these results is that, at a mass loading of unity, the dispersed phase significantly modifies the time-averaged structure of the jet shear layer, and
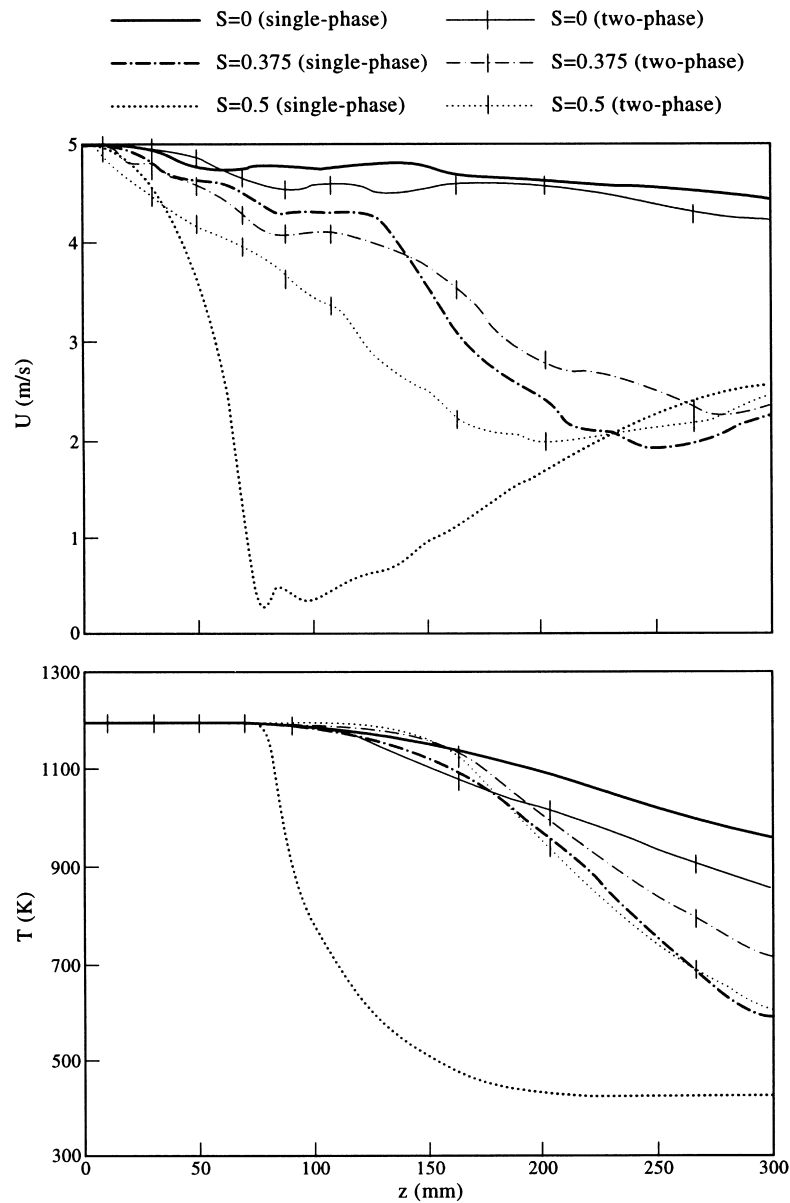

Figure 10. Axial profiles of time-averaged gas velocity and temperature for a swirling jet without and with two-way momentum coupling for different swirl numbers..
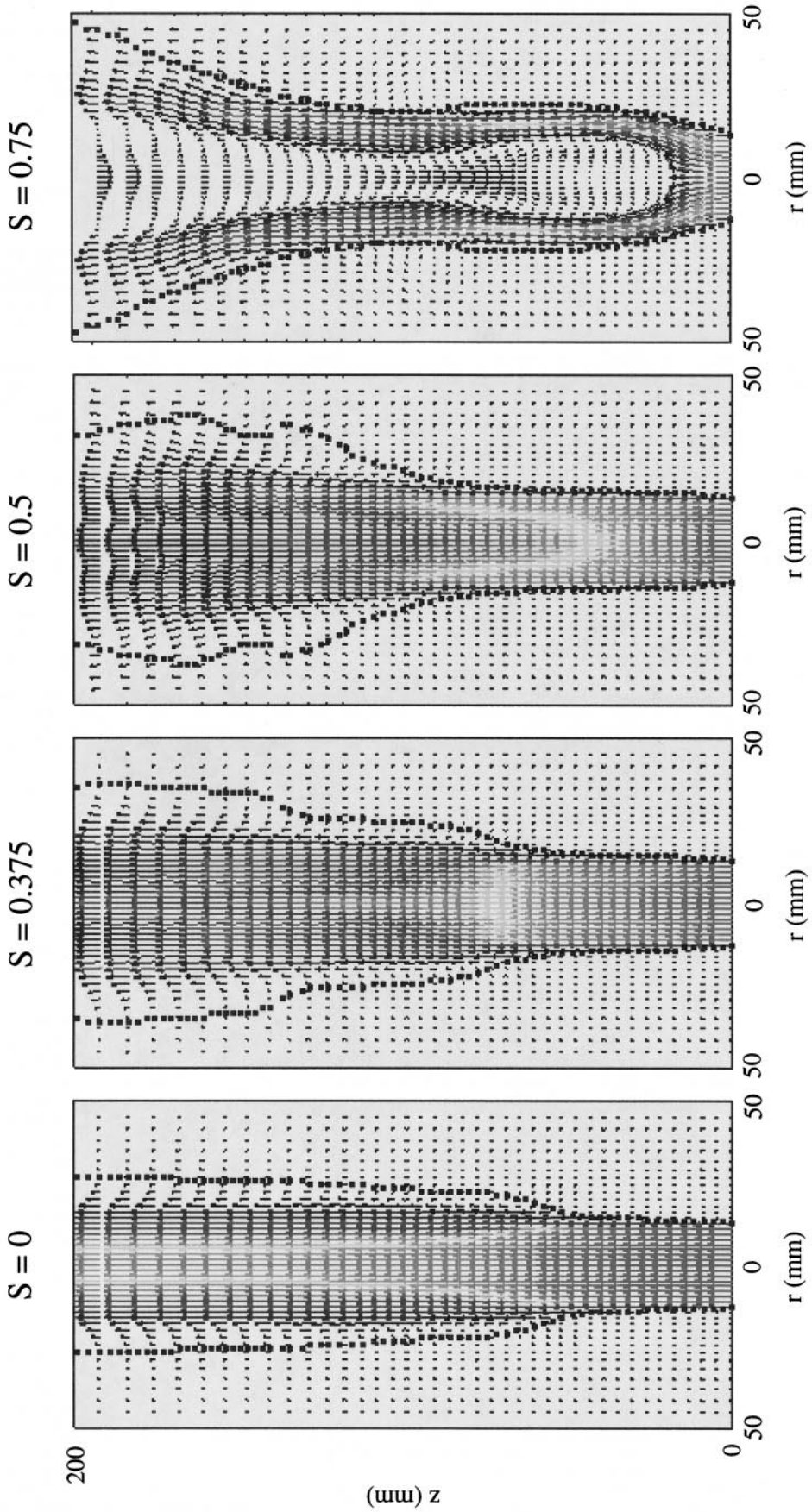
Figure 11. Time-averaged velocity vector plots for a two-phase swirling jet for different swirl numbers.

the degree of modification depends on the swirl intensity. For the nonswirling jet ($S = 0$), as the shear layer develops, the gas-phase velocity decreases along the centerline. Since the droplets are injected at the jet velocity, they now have higher velocity than the gas phase, resulting in a transfer of momentum from the dispersed phase to the gas phase. This seems to enhance the shear layer instability, resulting in enhanced mixing and entrainment of colder fluid, as evidenced by a faster decay of centerline temperature and velocity for the two-phase jet compared to those for the single-phase jet. This effect is modified significantly by the introduction of swirl. As noted earlier, the addition of swirl ($S = 0.375$) to a single-phase jet causes a faster decay of the centerline velocity (compared to a nonswirling jet), resulting in vortex pairing. This leads to enhanced mixing and entrainment of colder fluid into the shear layer; note a sharp increase in the rate of decrease of centerline velocity near an axial location of 120 mm for the single-phase jet. For the corresponding two-phase jet, the transfer of azimuthal momentum from the gas phase to droplets reduces the swirl intensity near the nozzle. This initially ($z < 120$ mm) causes a faster decay of centerline velocity for the two-phase jet compared to that for the single-phase jet. Further downstream, however, the direction of azimuthal momentum transfer is reversed, resulting in a slower decay of centerline velocity for the two-phase jet. In addition, the absence of vortex pairing for two-phase jet further reduces the rate of decay of centerline velocity. Consequently, the centerline velocity of two-phase jet becomes higher than that of single-phase jet for $z > 120$ mm. The absence of vortex pairing also results in reduced mixing and entrainment for the two-phase jet. Consequently, as indicated in figure 10(b), the centerline temperature decreases less rapidly for the two-phase jet.

The above effects become progressively stronger as the swirl number is increased. For $S = 0.5$, as shown in figure 10(a), the centerline velocity of single-phase jet first decreases quite rapidly due to the combined effects of shear layer growth, adverse pressure gradient, and vortex pairings, and then ($z > 100$ mm) increases due to the transfer of axial momentum in the radial direction; see also figure 6. For the corresponding two-phase jet, the centerline velocity decreases much less rapidly, again due to the reduced pressure gradient and the absence of vortex pairings. The centerline temperature also decreases slowly for the two-phase jet, again implying reduced mixing and entrainment due to the momentum coupling effect. Another effect of momentum coupling is seen from the comparison of time-averaged velocity vectors for single-phase and two-phase jets given in figures 6 and 11, respectively. The comparison of these figures shows that, due to the momentum transfer from droplets to gas phase in the jet shear layer, the jet width is decreased and the potential core is lengthened for the swirling two-phase jet. The effect becomes more distinguishable for $S = 0.5$ and 0.75, where the momentum coupling generates a curtain (or envelope) of high-velocity narrow region inside the shear layer. An important consequence of this high-velocity curtain is the near disappearance of the stagnation region for swirling two-phase jet for $S = 0.5$, and that of recirculation bubble for $S = 0.75$. The presence of a large recirculation bubble is perhaps the most distinguishing feature of a strongly swirling ($S = 0.75$) single-phase jet; see figures 3 and 6. For the corresponding two-phase jet, our results indicate that the recirculation bubble becomes nearly non-existent, even though the central stagnation and reverse flow regions still exist inside the high-velocity curtain. The disappearance of recirculation bubble for the strongly swirling case may be attributed to the momentum coupling effect, i.e. the transfer of various momentum components between the phases. Initially, there is a transfer of swirl momentum from the gas phase to dispersed phase, causing swirling intensity to decrease much more rapidly for two-phase jet (case B) compared to that for single-phase jet (case A). At some downstream location, however, the direction of azimuthal momentum transfer reverses, since droplets have higher momentum there. Secondly, the jet spreading rate is reduced for case B due to the radial momentum transfer from the gas phase to the dispersed phase. In addition, there is a reverse transfer of axial momentum, i.e. from the dispersed phase to gas phase, since the gas-phase axial velocity decreases more rapidly than that of dispersed phase, generating the high-velocity curtain mentioned earlier. All of these effects, i.e. reduced entrainment, more rapid decay of swirl velocity initially, and increase of gas velocity, lead to a near disappearance of the recirculation bubble for the strongly swirling two-phase jet. Consequently, for strongly swirling jets ($S > 0.5$), the jet spreading angle, shear layer

growth and entrainment are reduced significantly due to the effect of interphase momentum coupling.

4. CONCLUSIONS

In this paper, we have investigated the effects of swirl and two-phase momentum coupling on the dynamics and structural behavior of a droplet-laden swirling jet. A direct numerical solver based on an Eulerian–Lagrangian formulation, but without any turbulence or subgrid model, has been employed to simulate the transient behavior of a transitional swirling jet. Numerical results have been shown to be grid-independent both in terms of the global predictions and the detailed spatio-temporal profiles of relevant gas-phase profiles at different swirl numbers. In addition, the predicted Strouhal number associated with the large-scale structures for the non-swirling jet has been shown to be in agreement with the available experimental data. Then, a detailed flow visualization based on numerical simulation has been used to examine the dynamics of large scale structures and their interactions with the droplets in weakly and strongly swirling jet shear layers. In addition, the effects of swirl and dispersed phase on the time-averaged jet structure have been characterized. Important observations are as follows.

Results for single-phase swirling jets indicate that the dynamics of large scale structures are strongly affected by the degree of swirl imparted to the incoming jet. For low and intermediate swirl intensities, the vortex rings roll up closer to the nozzle exit, their frequency increases, and pairing interactions become progressively stronger as the swirl number is increased. For example, there is one weak vortex merging near $z/D = 6$ for the nonswirling jet, and two vortex mergings near $z/D = 3$ and 5 for $S = 0.375$, while for $S = 0.5$ the vortex mergings become stronger and occur near $z/D = 2$ and 3, respectively. Consequently, the interaction of vortex rings with the swirling flow field gives rise to a mechanism, which seems to be responsible for the enhanced shear layer growth and entrainment, and has not been observed in previous studies. This may be an important result, with the implication that the addition of moderate swirl to a transitional jet modifies its vortex dynamics in a way that further enhances the beneficial effects of both swirl and vortex structures on shear layer growth. For a strongly swirling jet, the presence of a central stagnant zone and recirculation bubble causes a drastic increase in the jet spreading angle, and this has a rather dramatic effect on vortex dynamics. Detailed visualization of the shear layer dynamics indicates that, as the shear layer is shifted radially outward, a pair of counter-rotating toroidal vortices is generated periodically, and the eventual shear layer structure, including the location of recirculation bubble, is determined by the dynamic interactions of these structures with the stagnant zone and recirculation bubble.

Results for the two-phase swirling jet indicate that at a mass loading ratio of unity, the jet dynamics and structural characteristics are strongly modified by the interphase momentum coupling. Depending upon the amount of swirl imparted to the jet, the momentum coupling can cause varied and in some cases dramatic effects on the dynamic and time-averaged jet structure. For a nonswirling jet, the momentum coupling alters the dynamics of large vortex structures, modifying their roll-up location and frequency, and causing enhanced mixing and entrainment of colder fluid into the shear layer. In contrast, for weakly and moderately swirling jets, the momentum coupling reduces the amount of adverse pressure gradient, and suppresses the vortex pairing interactions. These effects are caused by the redistribution of gas-phase axial, radial, and swirl momentum components due to the dispersed phase, and lead to significantly reduced shear layer growth, mixing and entrainment rates for two-phase jets compared to those for single-phase jets. In addition, the correlation between vortex frequency and swirl number is modified due to momentum coupling. For example, the dominant vortex frequency of single-phase jets increases with increasing swirl number, while that of two-phase jets appears to be independent of S.

At high swirl numbers ($S > 0.5$), the effects of momentum coupling on the jet structure appears to be even more dramatic compared to those at moderate swirl numbers. Results for $S = 0.75$ indicate that momentum coupling can significantly modify the rate of decay of swirl

intensity, and increase the gas axial momentum in the jet shear layer, leading to a dramatic reduction in the size of recirculation bubble.

REFERENCES

Aggarwal, S. K., Park, T. W. and Katta, V. R. (1996) Unsteady spray behavior in a heated jet shear layer: droplet–vortex interactions. *Combustion Science and Technology* **113,** 429–450.

Chung, J. N. and Troutt, T. R. (1988) Simulation of particle dispersion in an axisymmetric jet. *J. Fluid Mech.* **186,** 199–222.

Crow, S. C. and Champagne, F. H. (1971) Orderly structure in jet dynamics. *J. Fluid Mech.* **48,** 547–591.

Dellenbach, P. A., Metzger, D. E. and Neitzel, G. P. (1988) Measurements in turbulent swirling flow through an abrupt axisymmetric expansion. *AIAA J.* **26,** 669–681.

Durst, F. and Wennerberg, D. (1991) Numerical aspects on calculation of confined swirling flows with internal circulation, computation of strongly swirling axisymmetric jets. *Int. J. Numr. Meth. Fluids* **12,** 203–224.

Hussain, Z. D. and Hussain, A. K. M. F. (1983) Natural instability of free shear layers. *AIAA J.* **21,** 1512–1517.

Kailasanath, K., Gardner, J. H., Boris, J. P. and Oran, E. S. (1989) Acoustic–vortex interactions and low-frequency oscillations in axisymmetric combustors. *J. Propulsion and Power* **5,** 24–36.

Katta, V. R., Goss, L. P. and Roquemore, W. M. (1994) . *Combustion and Flame* **96,** 60–74.

Leonard, B. P. (1979) A stable and accurate convective modelling procedure based on quadratic upstream interpolation. *Comput. Meth. Appl. Mech. Eng.* **19,** 59–98.

Leschziner, M. A. and Rodi, W. (1984) Computation of strongly swirling axisymmetric jets. *AIAA J.* **22,** 1742–1747.

Lilley, D. G. (1977) Swirling flows in combustion: A review. *AIAA J.* **15,** 1063–1078.

Longmire, E. K. and Eaton, J. K. (1992) Structure of a particle-laden Round Jet. *J. Fluid Mech.* **236,** 217–257.

Park, T. W., Aggarwal, S. K. and Katta, V. R. (1996) A numerical study of droplet–vortex interactions in an evaporating spray. *Int. J. Heat Mass Transfer* **39,** 741–754.

Ribeiro, M. M. and Whitelaw, J. H. (1980) Coaxial jets with and without swirl. *J. Fluid Mech.* **96,** 769–795.

Reynolds, W. C. and Bouchard, E. E. (1981) *The Effect of Forcing on the Mixing Region of a Circular Jet, Unsteady Turbulent Shear Layer Flows.* Springer, New York, pp. 401–411.

Shau, Y. R., Dolling, D. S. and Choi, K. Y. (1993) Organized structure in a compressible turbulent shear layer. *AIAA J.* **31,** 1398–1405.

Sommerfeld, M. and Qui, H.-H. (1993) Characterization of particle-laden, confined swirling flows by phase-doppler anemometry and numerical calculation. *Int. J. Multiphase Flow* **19,** 1093–1127.

Spalding, D. B. (1972) A novel finite difference formulation for difference expressions involving both first and second derivatives. *Int. J. Num. Methods Eng.* **4,** 551–559.

Subbarao, E. R. and Cantwell, B. J. (1992) Investigation of a coflowing buoyant jet–experiments on the effect of Reynolds number and Richardson number. *J. Fluid Mech.* **245,** 69–90.

Uthuppan, J., Aggarwal, S. K., Grinstein, F. F. and Kailasanath, K. (1994) Particle dispersion in a transitional axisymmetric jet: A numerical simulation. *AIAA J.* **32,** 2004–2014.

Yule, A. J. (1978) Large-scale structure in the mixing layer of a round jet. *J. Fluid Mech.* **89,** 413–432.